PHYSICAL REVIEW B VOLUME 22, NUMBER 12 15 DECEMBER 1980

Influence of defects on the electronic structure of zinc oxide surfaces

W. Göpel and U. Lampe
Institut für Physikalische Chemie der Universität, Callinstrasse 3-3A, D-3000 Hannover, Federal Republic of Germany
(Received 11 February 1980)

Intrinsic point defects were produced on ZnO ($10\bar{1}0$) surfaces by thermal treatment, uv illumination, and CO exposure. Electronic structure and thermodynamics of surface defects as well as their influence on charge-transfer reactions are discussed.

I. INTRODUCTION

Chemical reactions at semiconductor-gas interfaces, which generally involve changes in the concentration of free electrons, have been of interest for many years in the fields of chemisorption and catalysis, corrosion, semiconductor device technology, etc.

The present situation in understanding charge transfer during chemisorption is characterized by various theoretical approaches of different degrees of sophistication and a lack of detailed experimental results.[1-9] Experimental studies, however, have failed so far to verify quantitatively the dependence of charge transfer on surface barrier heights as it is expected from theoretical models. A detailed quantitative study recently published by Lagowski *et al.*[10] was performed under moderate vacuum conditions ($P > 10^{-1}$ Pa) only. Temperature dependence and absolute values of sticking coefficients of the system ZnO-O_2 determined in this work deviate strongly from results obtained in our earlier ultrahigh-vacuum (UHV) studies.[11,12] Most probably, the discrepancy is due to contaminations and/or surface defects. The drastic influence of intrinsic defects on electronic properties of ZnO surfaces is studied systematically in the present paper.

Intrinsic defects are thermodynamically stable in every solid at $T \neq 0$ K. Equilibrium surface concentrations ("coverages" Θ) of defects are expected to deviate from corresponding bulk values. This generally leads to band bending, changes in concentrations of free electrons at the surface and hence changes in rates of charge transfer during chemisorption or catalysis as a function of Θ.

Mainly for experimental reasons and in spite of their general importance, surface defects of compound semiconductors have not yet been studied systematically. We therefore started extensive work on a "prototype surface," i.e., ZnO ($10\bar{1}0$), on which surface defects can be studied under controlled conditions: ZnO ($10\bar{1}0$) does not irreversibly form surface compounds in the presence of residual gas which cannot be removed by thermal treatment under UHV conditions.[13] This surface exhibits well-defined surface-atom reconstruction and has negligible concentration of electronic surface states in the band gap.[12,14] Several earlier papers indicate the existence of donor-type of ZnO defects near the surface.[15,16]

The present study deals with surface defects of ZnO ($10\bar{1}0$) which will be produced by high-temperature treatment, by uv illumination, and by CO exposure. Definitions to characterize space-charge layers due to defects are given in Sec. II. After presenting experimental details and results in Sec. III, the discussion starts with geometric models of defects in ZnO (Sec. IV A). The following Sec. IV B deals with concentration profiles of defects near the surface. In Secs. IV C and IV D electronic structures and conductivities of bulk and surface ZnO are discussed. We conclude the discussion with a thermodynamic treatment of surface defects (Sec. IV E) and the correlation between surface defects and reactivity (Sec. IV F).

II. DEFINITIONS

In order to calculate space-charge layers due to donor-type surface defects, we, in a first approximation, assume that electrostatic potentials have a dependence on the space coordinate z normal to the surface only. In this case, uniform work functions ϕ and surface conductivities $\Delta\sigma$ can easily be correlated by means of solutions from the Poisson equation.

ϕ is given by electron affinity χ, conduction-band edge E_C, bulk Fermi level E_F, and band bending at the surface eV_s:

$$\phi = \chi + (E_C - E_F) - eV_s . \tag{1}$$

The surface conductivity $\Delta\sigma$ is defined by the deviation of the resistance R from the value R_0 in flat-band situation[17]:

$$\Delta\sigma = \sigma_\square - \sigma_b V_{\text{sample}} A^{-1} = l^2/A(1/R - 1/R_0) \tag{2}$$

with $\sigma_\square$ = sheet conductance, σ_b = bulk conductivity

given by elementary charge e, concentration of electrons n_b as well as defect electrons p_b and corresponding mobilities $\mu_{e(p)}$; l = length, V_{sample} = volume, and A = total side area of samples with uniform geometric cross sections. Neglecting conductivity in surface states (until now not observed experimentally, see, e.g., Ref. 9), the equation

$$\Delta\sigma = e(\bar{\mu}_{s,e}\Delta N + \bar{\mu}_{s,p}\Delta P) \tag{3}$$

holds. $\bar{\mu}_{s,e(p)}$ is the mean mobility of electrons (defect electrons) in the space-charge layer, ΔN the excess surface concentration of electrons[17]

$$\Delta N = \int_0^\infty [n(z) - n_b]\,dz\,, \tag{4}$$

and ΔP the corresponding concentration of defect electrons in space-charge layers with Debye lengths L_{Deb} small as compared to the sample thickness.

The correlation between band bending eV_s and the average charge density Q_{ss} at the surface is given by charge neutrality

$$Q_{ss} + Q_{sc} = 0\,. \tag{5}$$

Here,

$$Q_{sc} = \int_0^\infty \rho(z)dz \tag{6}$$

is the average space charge per unit area obtained from integration of the Poisson equation with z-dependent charge density ρ:

$$\frac{d^2V(z)}{dz^2} = -\frac{\rho(z)}{\epsilon\epsilon_0}\,. \tag{7}$$

III. EXPERIMENTAL RESULTS

Figure 1 shows techniques used in our work to identify surface defects. Most experiments were carried out in an extended Varian 120 low-energy electron diffraction–Auger electron spectroscopy (LEED-AES) system.[18] For details of ultraviolet photoemission spectroscopy (UPS) experiments see Ref. 14. Cleaning procedures of ZnO ($10\bar{1}0$) included moderate high-temperature sublimation (1050 K, 180 s under Langmuir conditions) and subsequent oxygen treatment (typically 10^{-4} Pa, 700 K, 10^4 s). High sublimation rates at $T > 1100$ K lead to irreversible changes in the surface structure.[19] Ar bombardment could be avoided in the absence of Ca impurities. This preparation yields optimum LEED pattern with negligible surface impurities as checked by AES and thermal desorption spectroscopy (TDS). In all experiments, not intentionally doped ("undoped") ZnO was used.

A. Formation of surface defects

1. Thermal desorption experiments

Typical TDS results of Fig. 2 indicate characteristic intervals of temperature for typical surface reactions: Point defects become experimentally observable above 700 K, where TDS of "stoichiometric" surfaces [i.e., ZnO ($10\bar{1}0$) with an ideal Zn:O ratio of 1] leads to excess O_2 desorption.[20] If rapid heating ($dT/dt \geq 10$ K s^{-1}) is stopped at temperatures $885 \leq T_{\text{act}} \leq 977$ K, the isothermal excess Langmuir desorption of O_2 decays with a characteristic relaxation time $\tau = 177 \pm 15$ s. "Coverages" Θ of excess Zn at the surface (i.e., "nonstoichiometry") can be determined from the excess

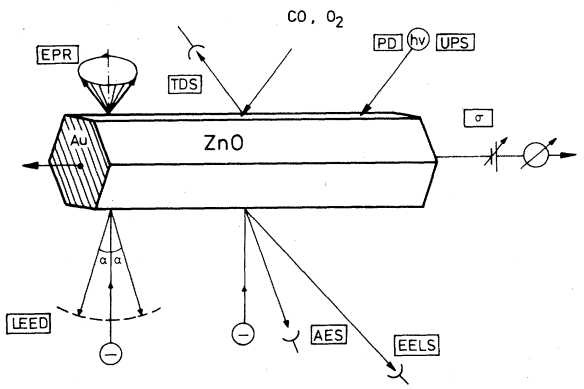

FIG. 1. Schematic diagram of experimental techniques: EPR (electron paramagnetic resonance), TDS (thermal desorption spectroscopy), PD (photodesorption), UPS [ultraviolet (He I, II) photoemission], σ (conductivity measurements), EELS (electron-energy-loss spectroscopy), AES (Auger electron spectroscopy), LEED LEED (low-energy electron diffraction).

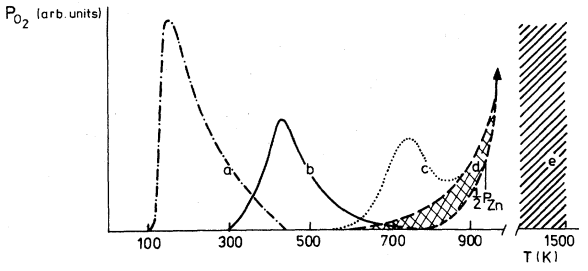

FIG. 2. Oxygen pressure during thermal desorption ($dT/dt = 3.3$ K s^{-1}). (a) After adsorption at $T_{\text{ads}} = 100$ K ["physisorption" with negligible change in surface conductivity (Refs. 12 and 13)]. (b) After adsorption at $T_{\text{ads}} = 300$ K ["chemisorption", formation of O_2^- at the surface (Refs. 11 and 13)]. (c) Desorption from nonideal (edge and kink) surface-atom positions during the first heating cycle of Ar-bombarded or chemically cleaned ZnO ($10\bar{1}0$). (d) Sublimation of the crystal. The upper slope is obtained during the first heating after chemisorption at 300 K. P_{O_2} in the hatched range is obtained on surfaces with different point-defect concentrations (Ref. 20). (e) High-temperature range of crystal preparation determining bulk defects in ZnO samples.

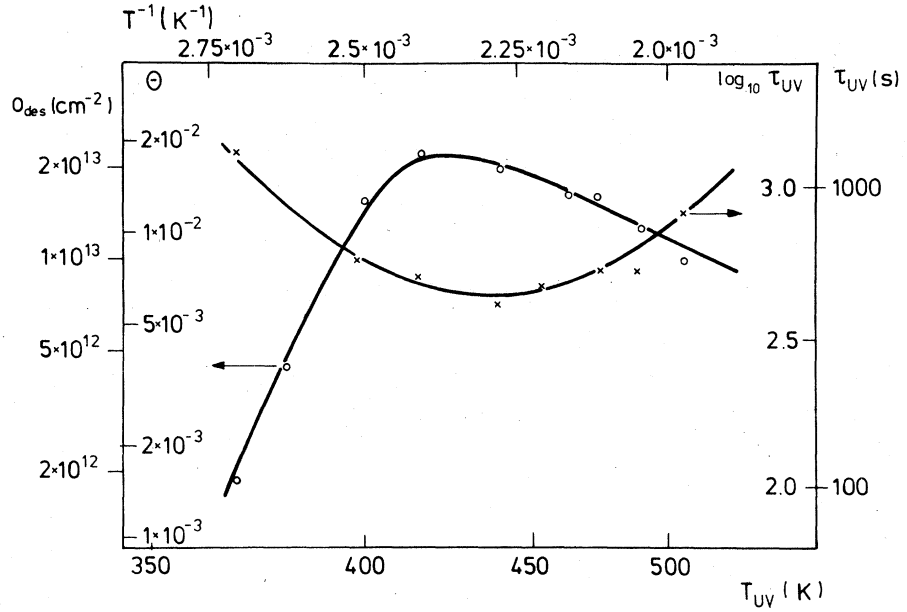

FIG. 3. Maximum excess surface concentration Θ of Zn determined from the amount of atoms O_{des} desorbing during uv illumination at T_{uv}. τ_{uv} is the characteristic relaxation time for decay of O atom desorption at T_{uv}.

amount of O_2 desorption at a given temperature ($10^{-4} \leq \Theta_{max}(T) \leq 10^{-2}$). Exponentially increasing Zn-sublimation rates with temperature are independent of Θ, whereas preexponential term $J_\infty(O_2)$ as well as activation energy $E_{subl}(O_2)$ of O_2 desorption both depend on Θ:

$$\ln J_\infty(O_2) = E_{subl}(O_2)/R \times 1002\ \text{K} + \ln J_{\infty,0}(O_2) \qquad (8)$$

with $0(\triangleq \Theta = 0) \leq E_{subl}(O_2) \leq 335 \pm 18$ kJ mol^{-1}[$\triangleq \Theta = \Theta_{max}(T)$] and $J_{\infty,0}(O_2) = 1.2 \times 10^{10}$ cm^{-2} s^{-1}.[20]

2. *Surface photolysis*

Surface defects may also be formed by uv illumination, which is known to cause a continous rise of surface conduction on ZnO single crystals.[15] In our experiments desorption of atomic oxygen could be observed during illumination with band-gap light (365 nm) at surprisingly low temperatures. At a given temperature, the amount O_{des} (Fig. 3) decays with characteristic relaxation times τ_{uv}. Evidently, the absolute values O_{des} may have large sys-

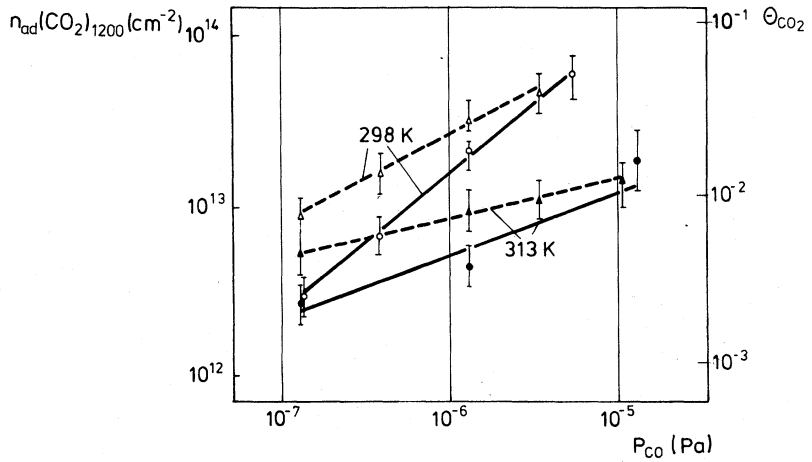

FIG. 4. Surface concentration n_{ad} (CO_2) of CO_2 formed after 1200-s CO exposure to ZnO ($10\bar{1}0$) at 300 K as determined from a subsequent TDS experiment. Circles: exposure to stoichiometric surfaces (pretreated at 700 K, $P_{O_2} = 10^{-4}$ Pa, $t = 10^3$ s), squares: exposure to surfaces with point defects (pretreated at $T_{act} = 950$ K, $P_{O_2,act} = 6.65 \times 10^{-5}$ Pa, corresponding to a point-defect concentration of 2.2×10^{13} cm^{-2}, compare Sec. IV E).

tematic errors. Relative values, however, from which τ_{uv} and the temperature dependence of O_{des} in Fig. 3 are deduced, could be reproduced within a few percent. The exponential increase of O_{des} below 400 K corresponds to an activation energy of about 70 kJ mol^{-1}. Photodesorption of O_2, H_2O, Zn, or CO was below detection limit. After CO exposure, however, CO_2 formation could be observed mass spectrometrically at 300 K in the presence of uv light.

3. *Surface reactions with CO*

In the absence of uv light, formation of surface defects due to CO exposure could indirectly be deduced from subsequent TDS, in which CO_2 was found. The TDS maximum temperature T_{max} is within experimental error identical with T_{max} of chemisorbed CO_2.[21] The dependence of $n_{ad}(CO_2)_{1200}$ on Θ as well as P_{CO} (Fig. 4) indicates complex kinetics and thermodynamics of ZnO-lattice oxidation at 300 K. For details see Ref. 22.

B. Conductivities as a function of temperature

Conductivity measurements are an extremely sensitive tool to determine quantitatively changes of electronic properties at the surface: After high-temperature formation of donor-type defects ("activation" of the surface at T_{act} and $P_{O_2,act}$ in range *d* of Fig. 2), characteristic changes were observed. For given T_{act} and $P_{O_2,act}$ σ was a unique function of the temperature below 750 K for different "activation times" $180 \leq t_{act} \leq 1600$ s and different cooling rates $0.8 \leq dT/dt \leq 8$ K s^{-1} after high-temperature "activation" (see typical results in Fig. 5). In these experiments, $P_{O_2,act}$ was reduced below 10^{-7} Pa after t_{act} at T_{act} within a few seconds to avoid "healing" up of defects due to O_2 reactions during cooling down to temperatures where defects are no longer stable (ranges *a* and *b* in Fig. 2, compare Secs. III C and IV F). The conductivity measurements indicate defects of donor type at the surface.

Particularly below 300 K the sheet conductance $\sigma_\square$ [Eq. (2)] shows drastic changes depending on

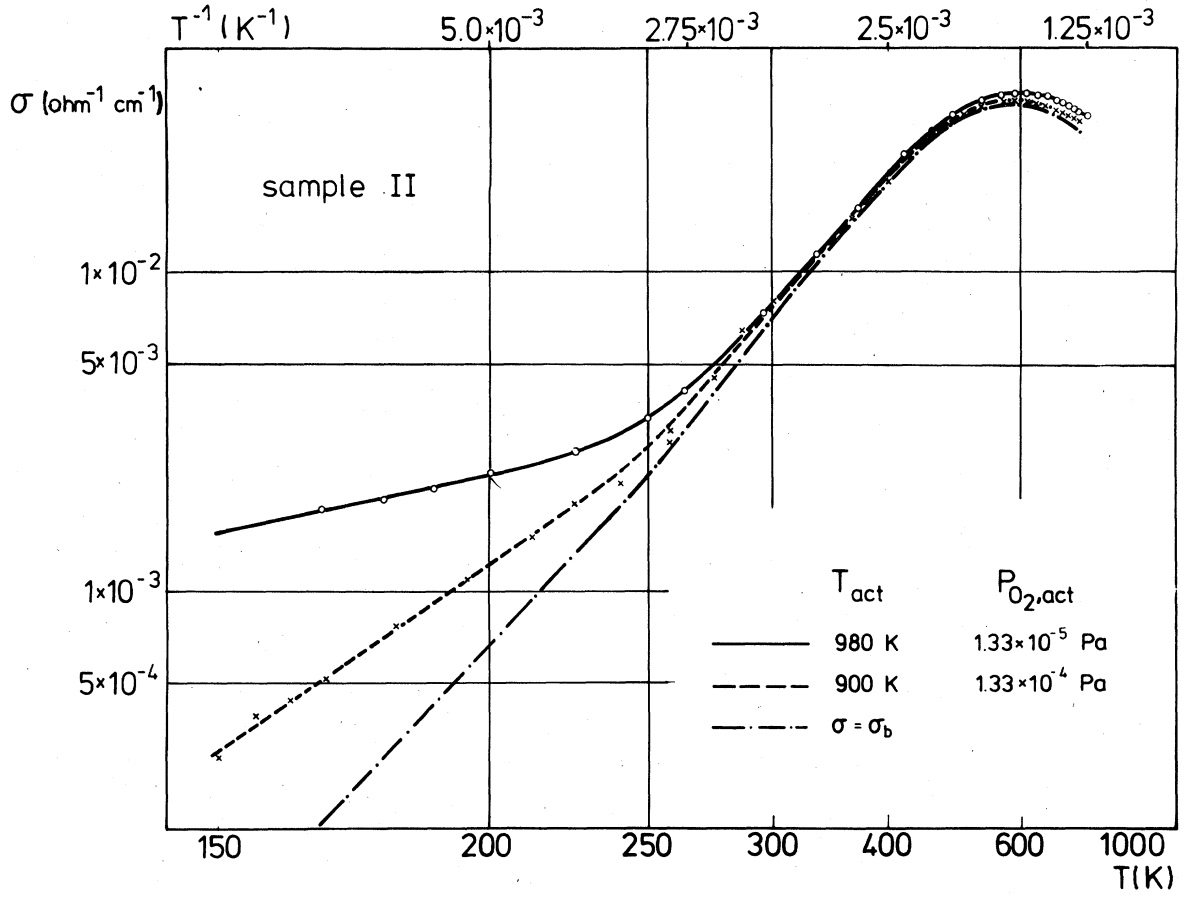

FIG. 5. Typical conductivities σ formally determined from $1/R$ of samples, which were pretreated in oxygen at T_{act} and $P_{O_2,act}$. $\sigma_b \sim 1/R_0$ was determined in the absence of point defects at the surface, i.e., $\Delta\sigma = 0$.

"activation" conditions (Fig. 6). In this range of temperature, mobilities are strongly influenced by scattering at ionized defects and by piezoelectric scattering.[23-40] Typical results are shown in Fig. 7 and Table I. Therefore, additional Hall measurements are needed to estimate donor concentrations from $\sigma_\square$. Above 500 K, however, unique μ_e values can be taken from the literature to calculate roughly mean concentrations of electrons n from our conductivity measurements assuming $\mu_e = \overline{\mu}_{s,e}$ (Fig. 8). $n_b = f(T)$, determined in the absence of surface defects as well as chemisorbed O_2, shows drastic variations for different ZnO samples (Fig. 9). This indicates different bulk electronic defects due to different preparation conditions (range e in Fig. 2) of ZnO samples and has to be taken into account in our theoretical calculations of space-charge layers (Sec. IV D).

The existence of donor-type surface defects also follows from conductivities of epitaxial thin films prepared on single-crystal Al_2O_3 substrates. Different values T_{act} and $P_{O_2,act}$ lead to different $\sigma_\square$ values extrapolated to $d = 0$ with unchanged slope, i.e., bulk contribution, for undoped samples (Fig. 10, for further details see Ref. 41). By means of $\mu_e = f(T)$ in Fig. 7, the $\sigma_\square(d \to 0)$ values can be used to determine excess surface concentrations of electrons ΔN from $\sigma_\square$ [Eqs. (2), (3), and (4), ΔP can be neglected for ZnO]:

$$\Delta N(P_{O_2,act}, T_{act}) = (1.1 \pm 0.2) \times 10^{15} P_{O_2,act}(\mathrm{Pa})^{-0.21 \pm 0.03} \times \exp[-(58 \pm 5)\ \mathrm{kJ\ mol^{-1}}/RT]\ \mathrm{cm^{-2}} \quad (9)$$

follows for undoped ZnO.

C. Conductivity changes upon O_2 exposure

If defects are produced by high-temperature treatment, by CO exposure and subsequent CO_2 de-

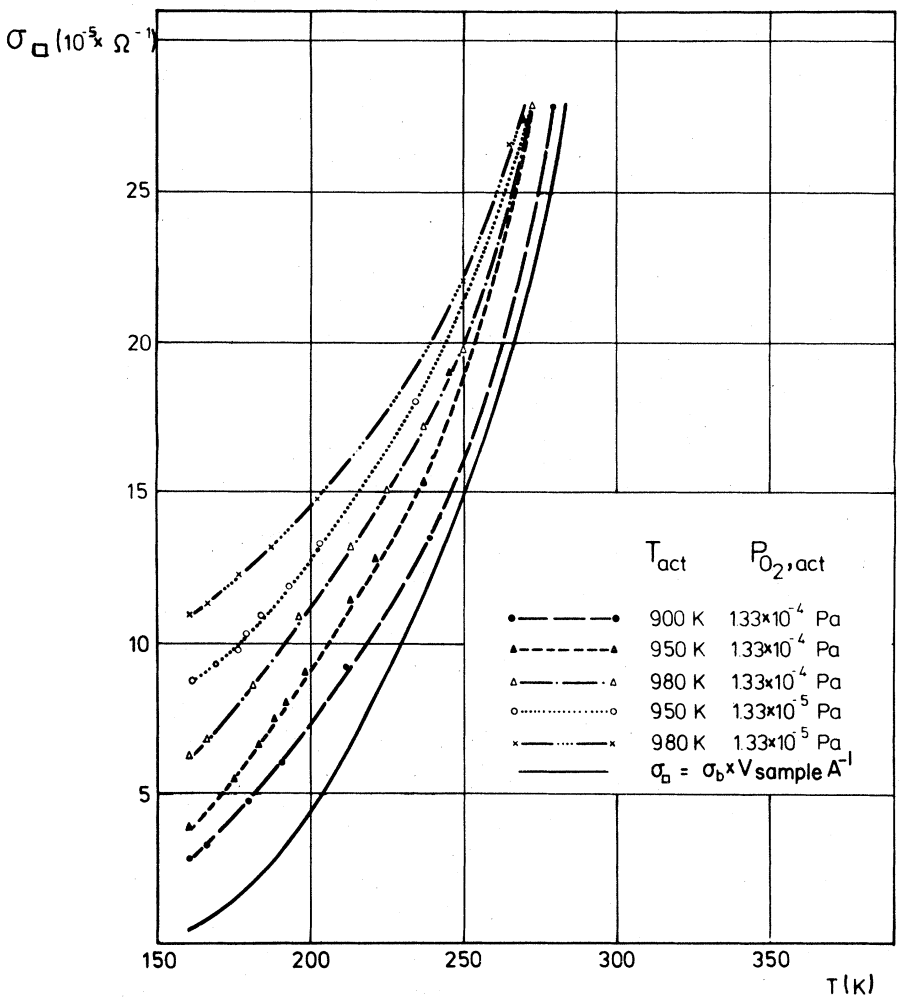

FIG. 6. Sheet conductance $\sigma_\square$ for different pretreatments at T_{act} and $P_{O_2 act}$.

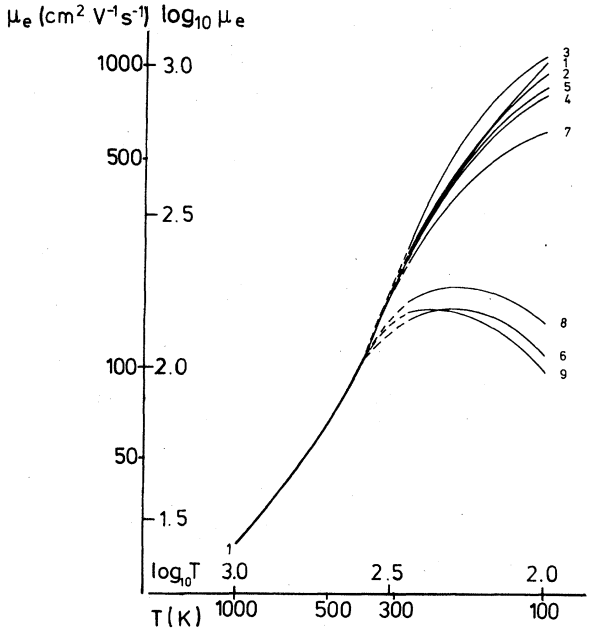

FIG. 7. Typical values for Hall mobilities μ_e of ZnO single crystals with different concentrations of bulk intrinsic defects (donor-type oxygen vacancies V_O and acceptor-type zinc vacancies V_{Zn}) and conductivities σ_b (taken from Refs. 23 and 24). Corresponding bulk concentrations of defects are given in Table I.

sorption, or by uv illumination, subsequent O_2 exposure at low temperatures $T \lesssim 700$ K leads to characteristic variations in conductivities. Total changes as well as initial slopes $(d\Delta\sigma/dt)_{t=0}$ during O_2 exposure can be used as a monitor to detect surface defects. Drastic changes in charge-transfer rates are observed, which are shown in Fig. 11 for thermally activated and in Fig. 12 for uv-activated samples ($P_{O_2} = 1.33 \times 10^{-4}$ Pa).

TABLE I. Bulk concentrations of donors (oxygen vacancies V_O) and acceptors (zinc vacancies V_{Zn}) as well as conductivities σ_b at 300 K for differently pretreated ZnO single crystals. Corresponding Hall mobilities μ_e are shown in Fig. 7.

Sample	$[V_O]$ (cm^{-3})	$[V_{Zn}]$ (cm^{-3})	σ_b (300 K) (Ω^{-1} cm^{-1})
1			1.0
2	3.5×10^{17}	1.4×10^{17}	1.4
3	9.4×10^{16}	4.3×10^{16}	0.24
4	3.65×10^{17}	1.4×10^{17}	1.8
5	4.16×10^{17}	1.75×10^{17}	1.4
6			7.3
7	4.4×10^{17}	1.25×10^{17}	4.3
8			50.7
9			62.7

D. AES, EELS, and LEED

Defects could not be observed in AES, e.g., by changed peak shapes or Zn:O peak intensities. Electron-energy-loss spectroscopy (EELS) enabled no fingerprint type of identification of surface defects. Experiments with better experimental resolution are highly desired. In LEED intensity I vs voltage U (I/U) curves, however, drastic changes were observed, which indicate long-range perturbations due to defects. Results for 0/0 spot intensities have been published previously.[21] The most prominent effect is an increase in the background intensity at 190 eV. Extra spots were never observed. Further experimental details are given in Ref. 12. LEED calculations on the basis of uniform variations in surface-atom reconstruction due to surface defects are in progress.[42]

E. Photoemission and electron paramagnetic resonance

In UPS, surface defects lead to reduced (O-2p derived) valence-band emission at 2–4 eV below the top of the valence band E_V. As in LEED, this effect indicates long-range perturbation. UPS details are given in Ref. 14.

In EPR, defects lead to an almost symmetric signal at $g = 1.9595$ which can be annihilated completely by low-temperature ($T < 700$ K) O_2 exposure. Relaxation times are of the order of minutes. If samples were pretreated over longer times ($t_{act} > 10^4$ s), a minor part of the $g = 1.9595$ signal is reduced with an order-of-magnitude longer relaxation time. This effect may indicate the different reaction rates with bulk and surface defects. Within experimental error, the same g value was observed for defects produced thermally, by uv illumination and by CO exposure. O_2 exposure below 400 K leads to an additional signal, which in our earlier work[12] had been attributed to an O_2^- surface complex.

IV. DISCUSSION

A. Geometric models of defects in ZnO

1. Bulk defects

Usual preparation conditions of zinc oxide single crystals lead to n-type conducting samples with excess Zn. This effect may formally be described by "nonstoichiometry" $Zn_{1+\delta}O$ ($\delta \lesssim 10^{-3}$) and/or structural disorder of ideal crystals due to point defects.

δ has been determined in x-ray,[43,44] channeling blocking,[45] or electrochemical measurements,[46,47] by gravimetric analysis,[48] hydrogen evolution,[49,50] and various chemical methods.[51-57] Attempts were

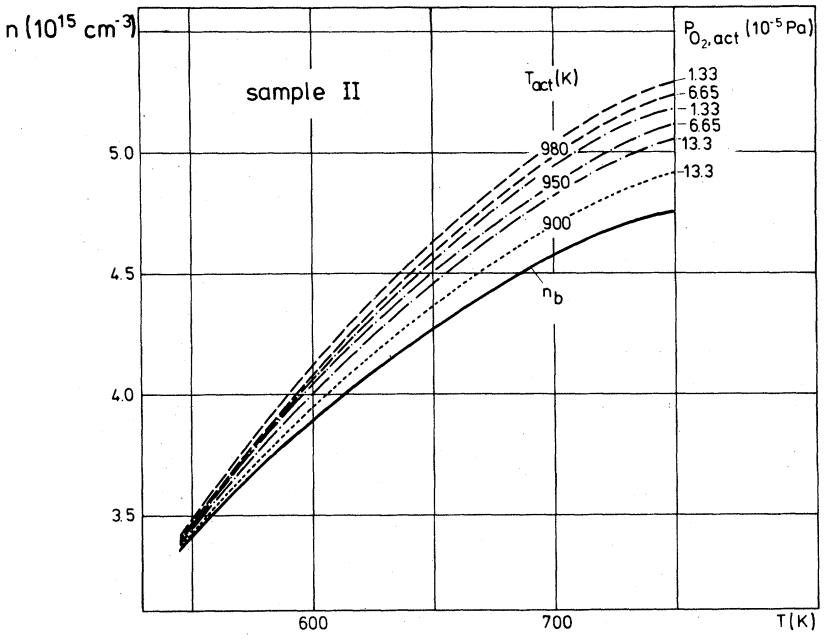

FIG. 8. Mean concentration of electrons n as function of temperature after high-temperature pretreatment of sample II at T_{act} and $P_{O_2,act}$. Further explanations are given in the text.

made to correlate "nonstoichiometry" with mobility and conductivity data.[47] The main problem in the quantitative determination of δ is to ensure homogeneity of defect concentrations in the sample. This problem will be discussed in Sec. IV B. "Segregation" of defects at the surface (Sec. IV D) had always been neglected in these studies.

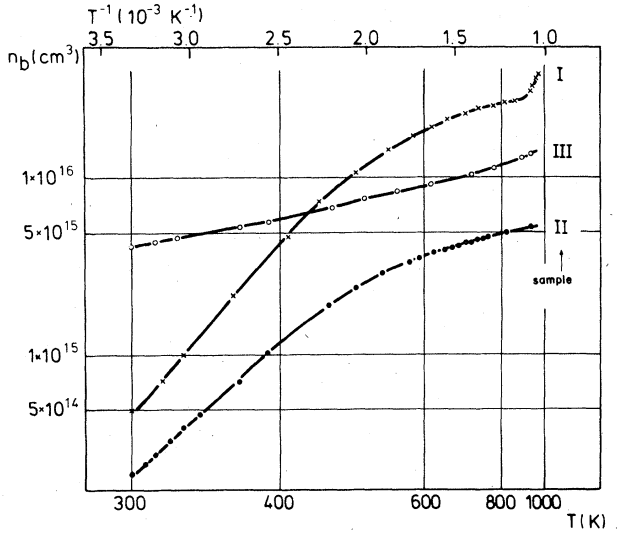

FIG. 9. Electron concentrations n_b as a function of temperature T determined from σ_b (compare Fig. 5) and μ_e (compare Fig. 7) for various ZnO samples.

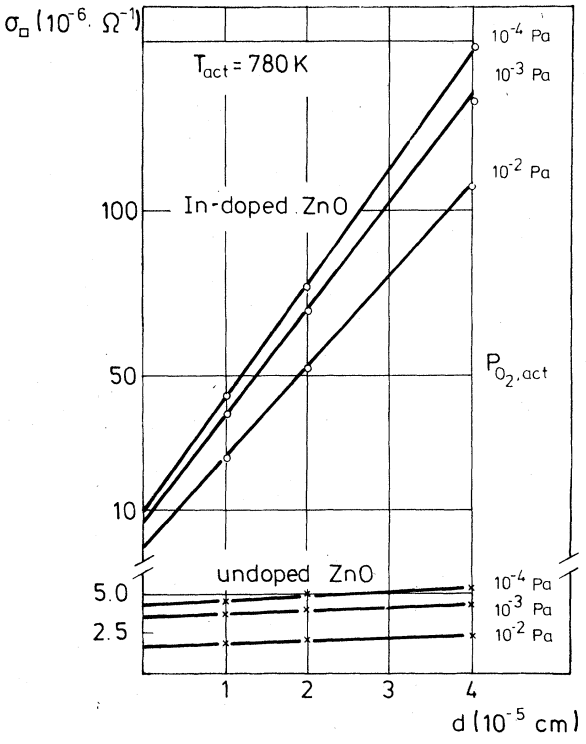

FIG. 10. Sheet conductance $\sigma_{\square}$ of epitaxial films measured at T_{act} as a function of film thickness d.

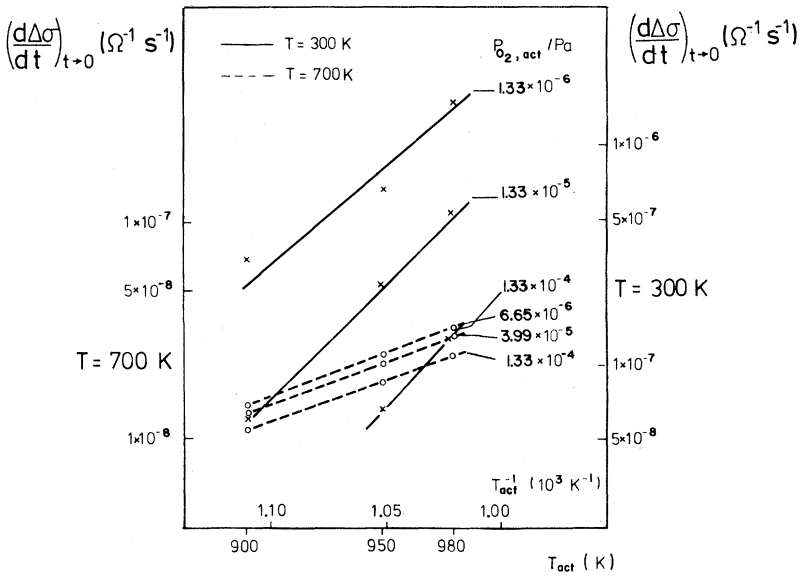

FIG. 11. Derivative of surface conductivity versus time during O_2 exposure extrapolated to $t=0$ for samples with different high-temperature pretreatments at T_{act} and $P_{O_2,act}$.

The physical origin of defects in bulk ZnO after various pretreatments is still not understood in detail. $\delta \neq 0$ may formally be explained by interstitial zinc Zn_i or oxygen vacancies V_O, both acting as donors. Diffusion and transport phenomena as well as conductivity data clearly show additional existence of acceptor types of defects, such as interstitial oxygen O_i or zinc vacancies V_{Zn}. A variety of experiments indicates the existence of V_O (Refs. 24–38, 45, and 58–71) and V_{Zn} (Refs. 24, 38, 60, and 72). Some authors found indications for Zn_i (Refs. 43, 45, 23, 60, 64, 65, 68, 70, and 72–75) and O_i (Refs. 61 and 69). Hagemark[39] discussed the coexistence of Zn_i and V_O. Theoretical calculations on the basis of an electrostatic polarization potential support the existence of V_O.[71]

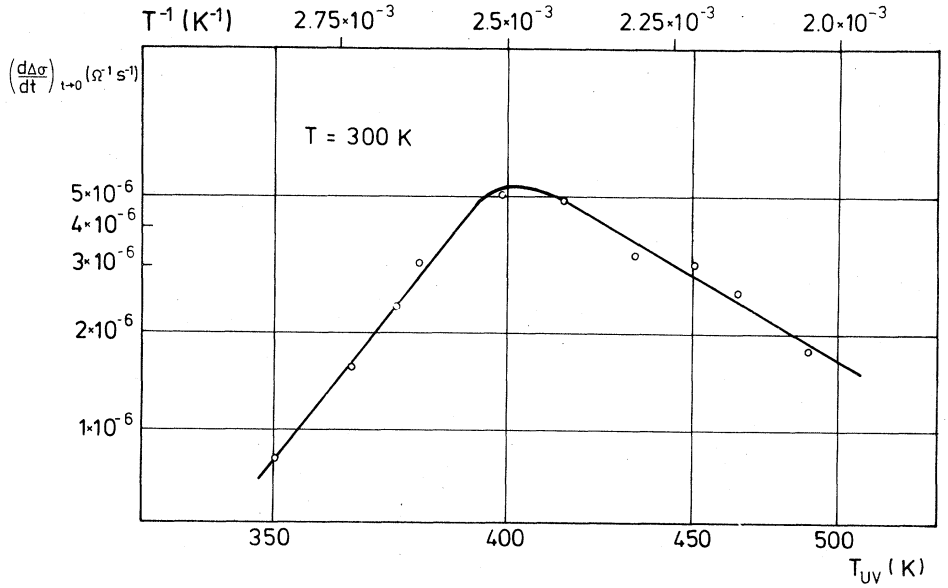

FIG. 12. Derivative of surface conductivity versus time during O_2 exposure extrapolated to $t=0$ for samples after uv illumination at T_{uv} ($t_{uv}=10^8$s).

A large number of coupled defect equilibria and temperature functions of corresponding equilibrium constants have been compiled without clearly identifying stabilities of different types of defects from high-temperature thermodynamics of bulk defects in ZnO (see, e.g., Ref. 60).

Various experimental results however, do indicate the existence of donor- as well as acceptor-type defects, both of which may be neutral, or singly- or doubly-ionized. The following discussion of electronic properties of ZnO will be simplified by assuming that V_O and V_{Zn} are the only donor and acceptor types of intrinsic defects in bulk ZnO (see Fig. 13). Their concentrations and energetic positions, estimated in Sec. IV C, determine the concentrations of free electrons, band bending due to surface defects (Sec. IV D), and hence charge-transfer reactions at the surface (Sec. IV F).

2. Surface defects

Surface defects of ZnO powders were often observed in EPR after thermal pretreatment,[66,67,69,76-78] or uv illumination with band-gap light.[79-82] A variety of earlier results on single crystals obtained by thermal or uv pretreatment,[15,16] by electron,[83-87] neutron[88] or proton[89] irradiation as well as our own results indicate donor-type paramagnetic surface defects.

The g value of our defects (Sec. III E) is, within experimental error, the same as the value obtained from ionized donors in the bulk after high-temperature pretreatment.[38,59] Spin-orbit coupling and geometrical surrounding of surface as well as bulk defects are therefore assumed to be the same. Following Hausmann,[38,59] we tentatively assign the signal to V_O and V_{O_s} (Fig. 13), respectively, and

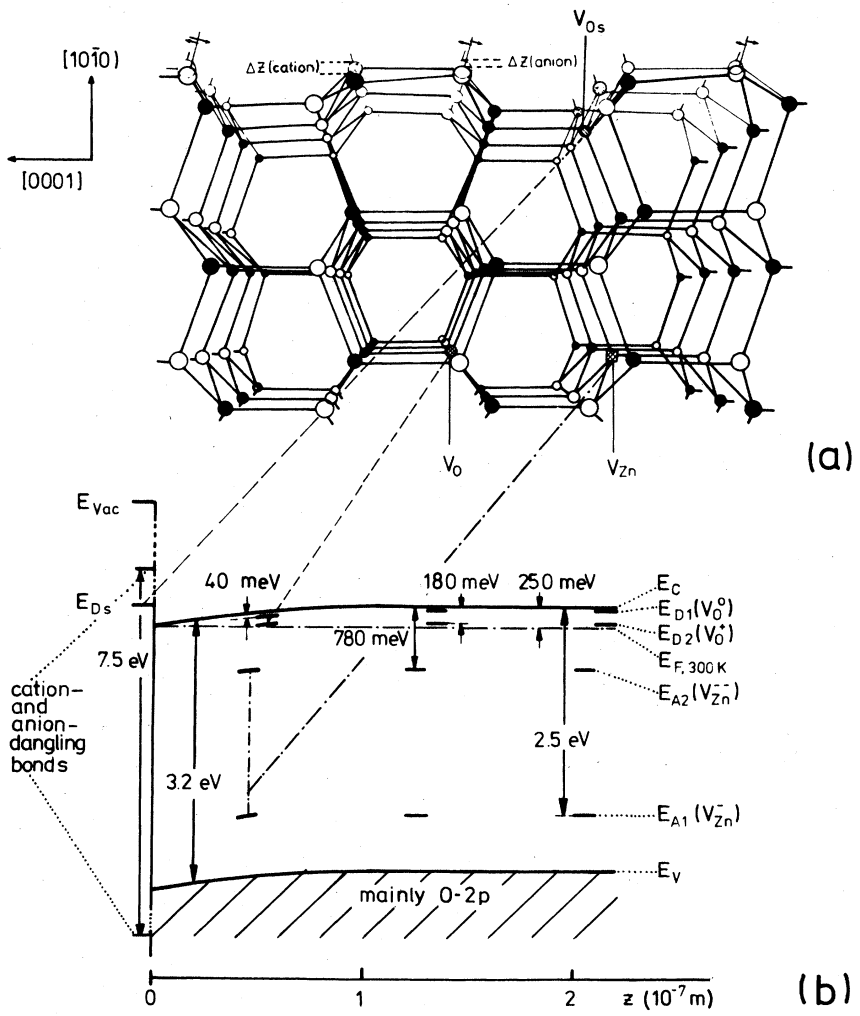

FIG. 13. Geometric model of ZnO with bulk and surface defects (a) and corresponding electronic structure (b). Energy values correspond to sample II at 300 K (for details see Sec. IV C).

we exclude Zn_{is} or V_{O_s} with three nearest neighbors at the surface. A proposed interpretation of the $g=1.9595$ signal in terms of free conduction electrons[79,82] may be excluded due to their rapid EPR relaxation. The different kinetics during reduction of the EPR signal upon O_2 exposure (Sec. III E) are assumed to raise from rapid reactions with V_{O_s} as compared to slow reactions with deeper lying V_O. Within experimental error, the same EPR signal (Sec. III E) and behavior upon low-temperature O_2 exposure (Sec. III C) is observed on surfaces with point defects, no matter if the defects were produced by thermal treatment, by uv illumination, or by CO exposure. We therefore tentatively assume that the same type of defect is produced in all cases. We also exclude acceptor-type surface defects, such as O_{is} or V_{Zn_s}. This assumption is supported by the facts that absolute values of conductivities of defect-free surfaces could be regained after O_2 exposure and EPR gave no indication for defects other than $V_{O(s)}$.

B. Concentration profile of defects near the surface

The concentration of bulk defects is given by preparation conditions of the single crystal at $1300 \lesssim T_{prep} \lesssim 1600$ K (range e in Fig. 2). We observed surface defects below 1000 K, where equilibrium concentrations of bulk defects per unit area are orders of magnitude smaller than concentrations of surface defects.[60] Bulk diffusion, however, is kinetically hindered at $T \lesssim 1000$ K. Quantitative estimations of diffusion effects are complicated by the fact that a unique picture about diffusion mechanisms in ZnO cannot be given at present. Experimental values, e.g., for chemical diffusion coefficients of oxygen, vary between $10^{-22} \lesssim D \lesssim 10^{-16}$ $cm^{-2}\,s^{-1}$ at $T=1000$ K (Refs. 90–93), and a similar variety of diffusion coefficients was determined for oxygen tracer diffusion and for diffusion of Zn.[94] In all cases, however, the expected mean displacement of defects is at most a few atomic distances under experimental conditions of our work. This is supported by the experimental fact that unique results for conductivities and conductivity changes (Figs. 5, 6, 8, and 10) could be obtained for high-temperature treatment at a given $P_{O_2,act}$ and T_{act} and various "activation times" (Sec. III B). Also, different cooling rates led to the same σ values after high-temperature treatment. Further on, our thin-film results clearly indicate surface effects (Fig. 10, Sec. III B).

We therefore conclude that extremely low bulk equilibrium concentrations of defects at $T<1000$ K are obtained at a distance from the surface, which is small as compared to the Debye length, whereas the majority of bulk defects remains unaffected, i.e., is "frozen in" under UHV conditions. Surface defects, however, which are stable in range d of Fig. 2 can only be "frozen in" in the absence of O_2, since they react rapidly with oxygen even at low temperatures ($T \lesssim 700$ K, compare Sec. IV F).

C. Electronic structure and conductivity of bulk ZnO

Recent studies of Heiland and Kohl[16] showed the necessity of taking into account compensation in interpreting surface phenomena of Cu-doped ZnO. Three bulk levels were formally determined to explain bulk conductivities and to calculate space-charge layers. A degeneracy of 16 was attributed to deep-lying (probably Cu) acceptor levels.[95] The physical origin of this defect, however, is not clear at present.

For our investigations on not intentionally doped ZnO we will try to correlate thermodynamic results of bulk defects with bulk electronic properties of our samples. The following concept can be applied to every compensated semiconductor with neutral and singly and doubly occupied donor as well as acceptor levels.

The ionization of defects is given by equilibrium constants taking into account Fermi statistics and degeneracy factors g_i.[96-97] $g_i=\frac{1}{2}$ (2) holds for ionization of doubly (singly) occupied defects N_D^+ (N_D^{++}) and $g_i=2$ ($\frac{1}{2}$) for N_A^- (N_A^{--}). If we further on introduce the conditions of electroneutrality as well as constant total concentrations of donors $N_D=N_D^0+N_D^+ +N_D^{++}$ and acceptors $N_A=N_A^0+N_A^-+N_A^{--}$, this leads to

$$\frac{N_D k_{D1}}{n_b^2+n_b k_{D1}+k_{D1}k_{D2}}\left(2k_{D2}+\frac{n_b^2+n_b k_{D1}}{k_{D1}+n_b}+\frac{k_i}{n_b}\right) = \frac{n_b N_A}{n_b^2+n_b k_{A2}+k_{A1}k_{A2}}\left(2n_b+\frac{k_{A1}k_{A2}+n_b k_{A2}}{k_{A1}+n_b}\right)+n_b \tag{10}$$

with[95]

$$k_i=n_b p_b=N_C N_V \exp[-(E_C-E_V)/kT]\,, \tag{11}$$

E_C and E_V are the conduction- and valence-band edges. N_C is the density of states in the conduction band if parabolic bands are assumed with $m_{eff}=0.28m_0$ (Ref. 98) and m_0 = free-electron mass. N_V is the corresponding density of states in the valence band with $m_{eff}=m_0$.

The equilibrium constants $k_{D1(2)}$ are given by

$$k_{D1}=N_D^+ n_b/N_D^0=g_{D1}N_C \exp[-(E_C-E_{D1})/kT]\,, \tag{12}$$

$$k_{D2}=N_D^{++} n_b/N_D^+=g_{D2}N_C \exp[-(E_C-E_{D2})/kT]\,, \tag{13}$$

TABLE II. Position of donor levels $E_{D1(2)}$ and acceptor levels $E_{A1(2)}$ and corresponding concentrations of donors N_D and acceptors N_A in the bulk of ZnO samples used in this work.

	Sample I	Sample II	Sample III
$E_C - E_{D1}$ (eV)	0.04	0.04	0.04
$E_C - E_{D2}$ (eV)	0.190	0.180	0.350
$E_C - E_{A2}$ (eV)	0.780	0.780	0.574
$E_C - E_{A1}$ (eV)	2.500	2.500	2.500
N_D (cm^{-3})	1.663×10^{17}	4.080×10^{17}	1.40×10^{16}
N_A (cm^{-3})	1.522×10^{17}	4.055×10^{17}	1.10×10^{16}

with $E_{D1,2}$ = first and second ionization level of donors. In analogy to $k_{D1,2}$, equilibrium constants $k_{A1,2}$ are given by acceptor levels $E_{A1,2}$ and corresponding degeneracy factors.

The general equation (10) can only be solved numerically, e.g., by fitting parameters to experimental results $n_b(T)$ in Fig. 9. Some ZnO parameters may be taken from the literature: $E_C - E_V = 3.2$ eV follows from Ref. 99. A first ionization level of acceptors $E_C - E_{A1} = 2.5$ eV was determined in Ref. 60. Shallow donor levels of higher concentration than acceptor levels always lead to n-type conductivity in compensated ZnO. The determination of bulk defects can be simplified further for some samples: For crystal I, in particular, a linear dependence of $\log n = f(1/T)$ at $T > 900$ K and $T < 400$ K indicates the prevailing contribution of one type of defect with corresponding energy E_{A2} and E_{D2}, respectively. The sets of parameters given in Table II allow a description of the bulk electronic structure of different samples used in this study over a wide range of temperatures. This is necessary for the calculation of space-charge layers in Sec. IV D.

D. Electronic structure and surface conductivity of ZnO ($10\bar{1}0$)

The bulk-defect levels and concentrations of Table II will be used to calculate band bending in depletion and accumulation layers with limitation to a nondegenerate conduction band, i.e., $E_C - E_F > 0$ at the surface. The degenerate case will only be estimated roughly according to calculations by Krusemeyer.[100] Deviations due to local electric fields with additional x and y dependence (see e.g., Ref. 101) as well as effects due to quantized subbands[102-105] will be neglected to first approximation.

The concentration of space charge is given by

$$\rho(z) = -e[n(z) + 2N_A^{--}(z) + N_A^{-}(z) - p(z) - 2N_D^{++}(z) - N_D^{+}(z)] + e(n_b + 2N_A^{--} + N_A^{-} - p_b - 2N_D^{++} - 2N_D^{+}). \tag{15}$$

For simplification, we assume $N_A^0 = 0$ (since $E_C - E_{A1} \gg E_C - E_F$) and $N_D^0 = 0$ (since $E_C - E_{D1} < kT$ for $T > 300$ K and limitation to calculation of nondegenerate conduction band). Fermi statistics control the occupation of different donor and acceptor levels at a given band bending $eV(z)$.

Substitution of $V = kTv/e$ and integration of the Poisson equation leads to

$$\frac{dv}{dz} = \pm\{2e^2(\epsilon\epsilon_0 kT)^{-1}[n^* + 2N_A^{*--} + N_A^{*-} - p^* - 2N_D^{*++} - N_D^{*+} - v(n_b + 2N_A^{--} + N_A^{-} - p_b - 2N_D^{++} - N_D^{+})]\}^{1/2} \tag{16}$$

with

$$n^* = N_C[v + \ln(1 + \exp\{[(E_C - E_F)/kT] - v\}) - \ln\{1 + \exp[(E_C - E_F)/kT]\}], \tag{17}$$

$$N_D^{*++} = -N_D[\ln(1 + \tfrac{1}{2}\exp\{[(E_{D2} - E_F)/kT] - v\}) - \ln\{1 + \tfrac{1}{2}\exp[(E_{D2} - E_F)/kT]\}], \tag{18}$$

$$N_D^{*+} = N_D[v + \ln(1 + \tfrac{1}{2}\exp\{[(E_{D2} - E_F)/kT] - v\}) - \ln\{1 + \tfrac{1}{2}\exp[(E_{D2} - E_F)/kT]\}] \tag{19}$$

and analogous expressions for N_A^{*-}, N_A^{*--}, and p^*. Surface densities of charge Q_{ss} [Eq. (5)] can be estimated from Eq. (16) by means of

$$Q_{ss} = \epsilon\epsilon_0 kTe^{-1}\left(\frac{dv}{dz}\right)_{z=0} = \epsilon\epsilon_0\left(\frac{dV_s}{dz}\right). \tag{20}$$

Characteristic results are shown in Fig. 14. The range of degenerate conduction bands in accumulation layers (thick lines) was estimated from

$$Q_{ss} = [8\pi\epsilon\epsilon_0 e^{-2}h^{-3}(2m_{\text{eff}})^{3/2}(kT)^{5/2}]^{1/2} \times\{[(E_F - E_C)_{z=0}]/kT\}^{5/4}(2)15^{-1/2} \tag{21}$$

assuming negligible quantization in subbands and spherical bands near E_C.[100] Evidently, quantum effects are negligible below $Q_{ss} \approx 10^{12}$ cm^{-2}. More sophisticated calculations according to Eger *et al.*[103] lead to more than 20% deviation from the semiclassical limit in Eq. (20) at $eV_s/kT > 40kT$. A detailed discussion, however, is beyond the scope of this article.

The surface density of mobile electrons ΔN [Eq. (4)] can be determined from

$$\Delta N = \int_{v_s}^{0} [n(z) - n_b]\left(\frac{dz}{dv}\right)dv \tag{22}$$

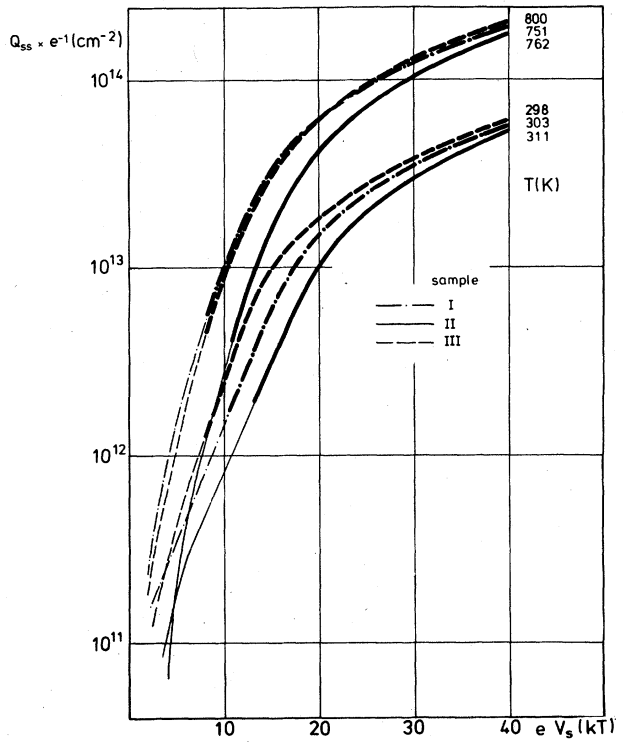

FIG. 14. Surface-charge density Q_{ss} of accumulation layers as function of band bending and temperature T. Thick lines correspond to degenerate conduction bands.

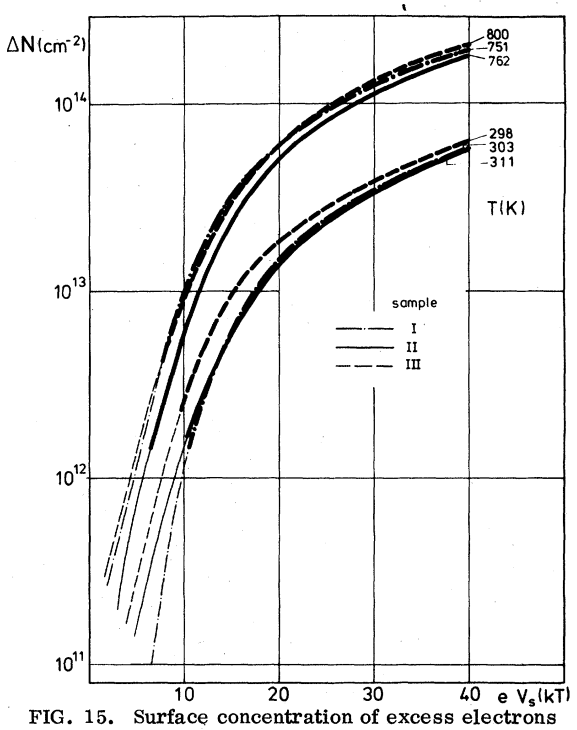

FIG. 15. Surface concentration of excess electrons ΔN in accumulation layers as function of band bending and temperature T. Thick lines correspond to degenerate conduction bands.

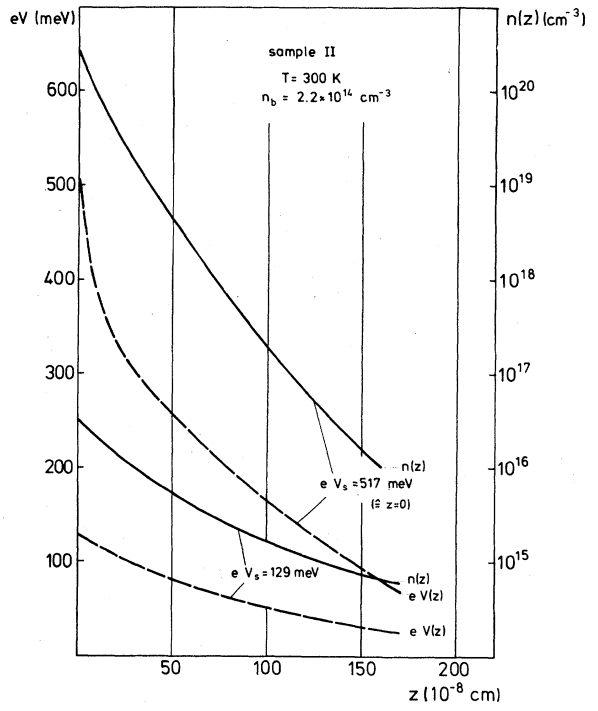

FIG. 16. Space dependence of $n(z)$ and $eV(z)$ in accumulation layers for different band bendings eV_s at the surface at $T = 300$ K. Further explanations are given in the text.

with $(dz/dv) = f^{-1}(z)$ from Eq. (16). Results obtained by numerical integration are shown in Fig. 15. In degenerate conduction bands $Q_{ss} = \Delta N$ was assumed.

Band-bending calculations are not affected by the unknown concentration profile of bulk defects in ZnO. Figure 16 shows the dependence of concentrations of free electrons and band bending as a function of distance from the surface. Results were obtained by numerical integration of Eq. (16). Under the experimental conditions of our work, the inhomogeneous doping due to bulk diffusion extends orders of magnitude less than accumulation layers (see typical results for 300 K in Fig. 16). We therefore conclude that our quantitative determination of surface charges and point defects from changes in free-electron concentrations is valid although inhomogeneous doping occurs near the surface of "real" ZnO single crystals.

The donor level of defects is located in the conduction band (Fig. 13). Our earlier studies, restricted to $T > 500$ K measurements, indicated a donor level 0.2 eV below E_C.[12] This value was formally deduced from the temperature dependence of typical results shown in Fig. 8. Besides variations in ΔN, the temperature dependence of mobilities, however, has to be taken into account, too:

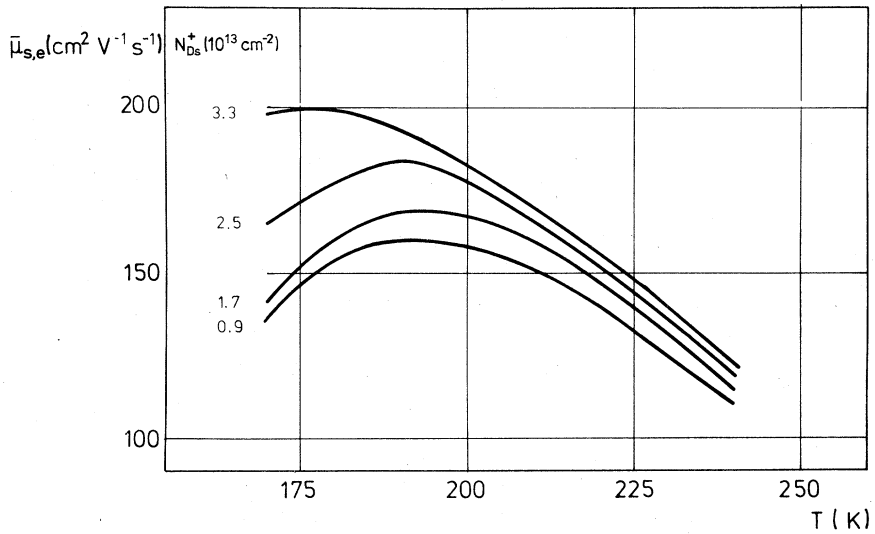

FIG. 17. Mean mobility $\bar{\mu}_{s,e}$ of electrons in accumulation layers of sample II after different high-temperature pretreatments at T_{act} and $P_{O_2,act}$ which lead to well-defined values $\Delta\sigma = f(T)$ and hence ΔN as well as N_{Ds}^+ (compare Fig. 18).

Deviations in differently doped samples become pronounced at low temperatures (compare Fig. 7). Therefore, only high-temperature ($T > 700$ K) results can be used to calculate ΔN from $\Delta\sigma$ under the assumption $\mu_e = \bar{\mu}_{e,s} \neq f(\Delta N)$.

If we assume complete ionization of defects, mean surface mobilities $\bar{\mu}_{s,e}$ can be estimated from $\Delta\sigma(T)$ data as a function of N_{Ds}^+. Results in Fig. 17 show qualitatively the same trend as bulk data with high defect concentrations due to excess zinc (Fig. 7, curves 6, 8, 9) and as those results in quantized accumulation layers on ZnO (Ref. 104) with a maximum at about 190 K. Increasing $\bar{\mu}_{s,e}$ with N_{Ds}^+ indicates cooperative scattering phenomena in strong accumulation layers. The concentration of ionized defects N_{Ds}^+ follows from $N_{Ds}^+ = Q_{ss} e_0^{-1}$. Results in Figs. 14 and 15 enable the determination of Q_{ss} from ΔN at a given band bending. In this way, thermally produced defect concentrations $N_{Ds}^+ = f(P_{O_2,act}, T_{act})$ and defect concentrations after uv illumination or CO exposure can be calculated from $\Delta\sigma$. Results are discussed in the following section.

E. Thermodynamics of surface defects

Defect concentrations due to surface preparation under thermodynamically controlled conditions at $T_{act}, P_{O_2,act}$ shown in Fig. 18 are formally given by

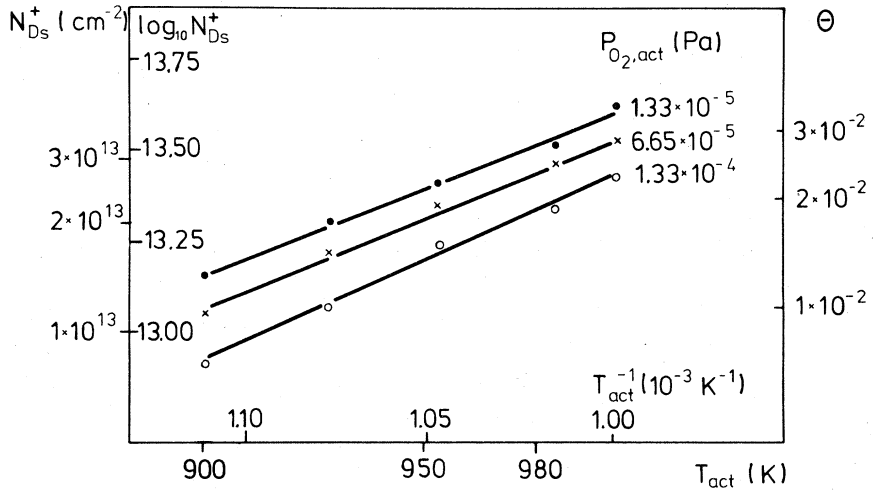

FIG. 18. Equilibrium concentration of surface donors N_{Ds}^+ as function of temperature T_{act} and pressure $P_{O_2,act}$.

$$N_{Ds}^{+} = (8.1 \pm 1) \times 10^{17} P_{O_2,\mathrm{act}}(\mathrm{Pa})^{-0.15 \pm 0.02} \times \exp[-(96 \pm 10)\ \mathrm{kJ\ mol^{-1}}/RT_{\mathrm{act}}]\mathrm{cm}^{-2}. \quad (23)$$

Small concentrations of defects, easily obtained under UHV conditions, induce degenerate accumulation layers (compare results in Figs. 15 and 18). As a result, "metallic surface conductivity" occurs at extremely low concentrations of surface defects. It is interesting to note that degenerate conduction bands with metallic surface conductivity occur under experimental conditions of catalytic oxidation reactions on ZnO.[106,107]

Absolute values N_{Ds}^{+} are of the order of ΔN values obtained on epitaxial thin films [Eq. (9)]. Deviations in preexponential and exponential terms are mainly due to deviations in the bulk concentration of intrinsic as well as extrinsic (In) point defects. Details will be discussed in a following paper.[41]

In a thermodynamic approach, the "defect unity" $V_{O_s}^{+} + e \rightleftarrows V_{O_s}^{0}$ may be treated as a "negatively adsorbed particle." Adsorption isotherms obtained from Eq. (23) enable the estimation of isosteric heats of "adsorption":

$$q_{st} = \left(\frac{\partial \ln P_{O_2\mathrm{act}}}{\partial T}\right)_{N_{Ds}^{+}} RT^2 \quad (24)$$

with $q_{st} = -640 \pm 40$ kJ mol^{-1}. Since q_{st} is the difference between molar enthalpies in the gas phase (which are well known) and in the "adsorption" state for the process

$$2O_L \rightleftarrows 2V_{O_s} + 2e + O_{2,\mathrm{gas}} ,$$

excess enthalpies and specific heats during formation of surface defects can be deduced from q_{st}.

F. Surface defects and reactivity

Rates of charge-transfer reactions can be drastically increased due to point defects at the surface. For a quantitative estimation of this effect, kinetic results in Figs. 11 and 12 were used to calculate the ratio S_0 of electrons captured from the conduction band per colliding O_2 molecule during low-temperature O_2 exposure. After determining N_{Ds}^{+} from $P_{O_2,\mathrm{act}}$ and T_{act} for thermally produced defects (compare Sec. IV D), results from Fig. 11 lead to

$$S_0(300\ \mathrm{K}) = 1.8 \times 10^{-6} \exp(5.0 \times 10^{-14} N_{Ds}^{+}/\mathrm{cm}^{-2}) \quad (25)$$

and

$$S_0(700\ \mathrm{K}) = 9.8 \times 10^{-6} + 2.77 \times 10^{-19} N_{Ds}^{+}/\mathrm{cm}^{-2} . \quad (26)$$

For "uv-activated" ZnO $(10\bar{1}0)$, results from Fig. 12 were calibrated assuming $N_{Ds}^{+} = O_{\mathrm{des}}$ (compare Fig. 3). Within experimental error, the same exponential dependence on N_{Ds}^{+} as in Eq. (25) was observed at 300 K. The exponential dependence at 300 K indicates chemisorbed O_2^- as precursor for reactions with V_{O_s}, whereas the linear slope at 700 K indicates direct reactions of O_2 with V_{O_s}. In both cases, isotopic exchange of $^{36}O_2$ has been observed for $N_{Ds}^{+} \neq 0$. This effect illustrates the important catalytic property of V_{O_s} to dissociate O_2 molecules even at low temperature.[107] Further details and implications for understanding the catalytic oxidation of CO on ZnO $(10\bar{1}0)$ will be discussed in a following paper.[108]

IV. CONCLUSIONS

Free energies of formation for surface defects are generally expected to deviate from bulk data. The present study on our "prototype system" ZnO $(10\bar{1}0)$ shows that equilibrium surface concentrations of intrinsic point defects may deviate significantly from corresponding bulk values. This effect leads to strong accumulation layers, orders of magnitudes larger concentrations of free carriers at the surface, drastic variations in rates of charge transfer, and hence a strong influence on catalytic properties.

ACKNOWLEDGMENTS

We would like to thank W. Seehausen for the experimental results on ZnO epitaxial films, Professor Dr. G. Heiland (Aachen) for donation of ZnO single crystals and the Deutsche Forschungsgemeinschaft, Fonds der Chemischen Industrie as well as Xerox Palo Alto (USA) for financial grants.

[1] P. Aigrain and C. Dugas, Z. Elektrochem. 56, 363 (1952).
[2] K. Hauffe and H. J. Engel, Z. Elektrochem. 56, 366 (1952).
[3] P. B. Weisz, J. Chem. Phys. 20, 1483 (1952); 21, 1531 (1953).
[4] S. R. Morrison, Adv. Catal. 7, 259 (1955); F. Garcia-Moliner, Catal. Rev. 2, 1 (1968).
[5] T. Wolkenstein, Adv. Catal. 12, 189 (1960); T. E. Madey, J. T. Yates, Jr., D. R. Sandstrom, and R. J. H. Voorhoeve, in *Treatise on Solid State Chemistry*, edited by N. B. Hannay (Plenum, New York, 1976), 6B, p. 59.
[6] A. Many, CRC Crit. Rev. Solid State Sci. 4, 515 (1974).

[7]S. R. Morrison, in *Surface Physics of Phosphors and Semiconductors*, edited by C. G. Scott and C. E. Reed (Academic, New York, 1975), p. 221.
[8]S. R. Morrison, in *Treatise on Solid Chemistry*, edited by N. B. Hannay (Plenum, New York, 1976), Vol. 6B, p. 203.
[9]See, e.g., M. Henzler, in *Surface Physics of Materials*, edited by J. M. Blakely (Academic, New York, 1975), Vol. 1.
[10]J. Lagowski, E. S. Sproles, Jr., and H. C. Gatos, J. Appl. Phys. 48, (8), 1566 (1977).
[11]W. Göpel, Ber. Buns. Ges. Phys. Chem. 80, 481 (1976).
[12]W. Göpel, J. Vac. Sci. Technol. 15, (4), 1298 (1978).
[13]W. Göpel, J. Vac. Sci. Technol. 16, (5), 1229 (1979).
[14]W. Göpel, R. S. Bauer, G. Hansson, Surf. Sci. 99, (1980).
[15]See, e.g., G. Heiland, Z. Phys. 148, 28 (1957); G. Heiland, E. Mollwo and F. Stöckmann, Solid State Phys. 8, 191 (1959); G. Heiland, J. Phys. Chem. Sol. 22, 227 (1961); D. Kohl and G. Heiland, Surf. Sci. 63, 96 (1977); H. Moormann, D. Kohl and G. Heiland, *ibid.* 80, 261 (1979).
[16]G. Heiland and D. Kohl, Phys. Status Solidi A 49, 27 (1978).
[17]See, e.g., A. Many, Y. Goldstein, and B. Grover, *Semiconductor Surfaces* (North-Holland, Amsterdam, (1971).
[18]W. Göpel, Surf. Sci. 62, 165 (1977).
[19]W. Göpel and G. Neuenfeldt, Surf. Sci. 55, 362 (1976).
[20]W. Göpel, Z. Phys. Chem. Neue Folge, 106, 211 (1977).
[21]W. Hotan, W. Göpel, and R. Haul, Surf. Sci. 83, 162 (1979).
[22]U. Lampe, thesis, University of Hannover (1979) (unpublished) and Conference Proceedings of the Eighth International Vacuum Congress, Cannes, 1980 (in press).
[23]A. R. Hutson, Phys. Rev. 108, 222 (1957).
[24]B. Utsch and A. Hausmann, Z. Phys. B 21, 27 (1975).
[25]H. Rupprecht, J. Phys. Chem. Sol. 6, 144 (1958).
[26]H. Chon and Ch. D. Prater, Discuss. Faraday Soc. 41, 380 (1966).
[27]H. Chon and J. Pajares, J. Catal. 14, 257 (1969).
[28]J. D. Zook, Phys. Rev. 136, A869 (1964).
[29]K. J. Hagemark and F. J. McFadden, Research Report 3M Co., 1970 (unpublished).
[30]G. Bogner, J. Phys. Chem. Solids 19, 235 (1961).
[31]G. Müller and R. Helbig, J. Phys. Chem. Solids 32, 1971 (1971).
[32]E. Mollwo, G. Müller and P. Wagner, Solid State Commun. 13, 1283 (1973).
[33]K. J. Hagemark, Research Report 3M Co., 1979 (unpublished).
[34]K. J. Hagemark, P. W. Li, J. Solid State Chem. 12, 371 (1975).
[35]A. Hausmann and W. Teuerle, Z. Phys. 257, 299 (1972).
[36]A. Hausmann and W. Teuerle, Z. Phys. 259, 189 (1973).
[37]K. J. Hagemark and L. C. Chacka, J. Solid State Chem. 15, 261 (1975).
[38]A. Hausmann and B. Utsch, Z. Phys. B 21, 217 (1975).
[39]K. J. Hagemark, J. Solid State Chem. 16, 293 (1976).
[40]R. Helbig and P. Wagner, J. Phys. Chem. Solids 35, 327 (1974).
[41]W. Seehausen, thesis, University of Hannover, 1978 (unpublished); W. Seehausen, W. Göpel, R. Haul, and U. Lampe, Conference Proceedings of the Eighth International Vacuum Congress, Cannes, 1980 (in press).
[42]A. Kahn, C. B. Duke, and W. Göpel (unpublished).
[43]A. Cimino, G. Mazzone, and P. Porta, Z. Phys. Chem. N. F. 41, 154 (1964).
[44]G. P. Mohanty and L. V. Azaroff, J. Chem. Phys. 35, 1268 (1961).
[45]B. R. Appleton and L. C. Feldman, J. Phys. Chem. Solids 33, 507 (1972).
[46]H. J. Engell, Z. Elektrochem. 60, 905 (1956).
[47]K. J. Hagemark and P. E. Toren, J. Electrochem. Soc. 122, 992 (1975).
[48]J. S. Choi and C. H. Yo, J. Phys. Chem. Solids 37, 1149 (1976).
[49]H. J. Allsopp, Analyst (London) 82, 474 (1957).
[50]H. J. Allsopp and J. P. Roberts, Nature (London) 180, 603 (1957).
[51]W. F. Ehret and A. Greenstone, J. Am. Chem. Soc. 65, 872 (1943).
[52]J. Deren and E. Fryt, Chem. Anal. (Warsaw) 8, 365 (1963).
[53]J. Deren and A. Kowalska, Chem. Anal. (Warsaw) 7, 563 (1962).
[54]V. J. Norman, Analyst (London) 89, 261 (1964).
[55]V. J. Norman, Aust. J. Chem. 19, 1133 (1966); 20, 85 (1967); 21, 299 (1968).
[56]J. M. Kruse, Anal. Chem. 43, 771 (1971).
[57]N. Dupont-Pavlowsky *et al.*, Phys. Status Solidi A 35, 615 (1976).
[58]J. Bogner, J. Phys. Chem. Solids 19, 235 (1961).
[59]A. Hausmann, Z. Phys. 237, 86 (1970).
[60]F. A. Kröger, *Chemistry of Imperfect Crystals* (North-Holland, Amsterdam, 1974).
[61]E. Mollwo, Phys. Rev. 162, 557 (1961).
[62]J. M. Meese, D. R. Locker, Solid State Commun. 11, 1547 (1972).
[63]T. Mookherij, Phys. Status Solidi A 13, 293 (1972).
[64]J. Schneider and A. Räuber, Z. Naturforsch. 16, 712 (1961).
[65]M. Seteka, Bull. Chem. Soc. Jpn. 43, 2377 (1970).
[66]K. Hoffmann, thesis (Freie Universität, Berlin, 1973 (unpublished).
[67]K. M. Sancier, J. Catal. 9, 314 (1966).
[68]P. P. Iyengar, J. Phys. Chem. 75, 3089 (1971).
[69]H. G. Fitzky, Photogr. Korresp. 103, 173 (1967).
[70]S. Harrison, Phys. Rev. 58, 52 (1954).
[71]W. F. Wei, Phys. Rev. B 15, 2250 (1977).
[72]P. G. Thomas, J. Phys. Chem. Solids 9, 31 (1959).
[73]R. E. Schrader and H. W. Lewerenz, J. Opt. Soc. Am. 37, 939 (1974).
[74]E. Scharowski, Z. Phys. 135, 318 (1953).
[75]G. P. Mohanty and L. V. Azaroff, J. Chem. Phys. 35, 1268 (1961).
[76]J. O. Cope and I. D. Campbell, Trans. Faraday Soc. 69, 1 (1973).
[77]M. Setaka, K. M. Sancier, and T. Kwan, J. Catal. 14, 44 (1970).
[78]K. Hoffmann and D. Hahn, Phys. Stat. Sol. A 24, 637 (1974).
[79]K. M. Sancier, Surf. Sci. 21, 1 (1970).
[80]G. K. Born *et al.*, Phys. Status Solidi A 4, 675 (1971).
[81]T. Mookherji, Phys. Status Solidi A 13, 293 (1972).
[82]K. M. Sancier, J. Phys. Chem. 76, 2527 (1972).
[83]J. M. Smith and W. E. Vehse, Phys. Lett. 31A, 147 (1970).

[84]C. Gonzalez, D. Galland, and A. Herve, Phys. Status Solidi B 72, 309 (1975).
[85]V. Soriano and D. Galland, Phys. Status Solidi B 77, 739 (1976).
[86]B. Schallenberger and A. Hausmann, Z. Phys. B 23, 177 (1976).
[87]A. Hausmann and B. Schallenberger, Z. Phys. B 31, 269 (1978).
[88]A. L. Taylor, G. Filipovitch, and G. K. Lindeberg, Solid Stat. Commun. 8, 1359 (1970).
[89]M. J. Duck and R. L. Nelson, Trans. Faraday Soc. 70, 436 (1974).
[90]J. W. Hoffmann, and F. Lauder, Trans. Faraday Soc. 66, 2346 (1970).
[91]W. J. Moore and F. L. Williams. Discuss. Faraday Soc. 28, 86 (1959).
[92]R. Robin, A. R. Cooper, and A. H. Heuer, J. Appl. Phys. 44, 3770 (1973).
[93]D. Hallwig and H. G. Sockel, in Achtes Killoquium über metallkundliche Analyse mit besonderer Berücksichtigung der Elektronen- und Ionenstrahlanalyse, Wien, 1976 (unpublished).
[94]P. Kofstad, *Nonstoichiometry, Diffusion, and Electrical Conductivity in Binary Metal Oxides* (Wiley, New York, 1972); D. A. Stevenson, in *Atomic Diffusion in Semiconductors*, edited by D. Shaw (Plenum, New York, 1973), Chap. 7; R. Lindner, Acta Chem. Scand. 6, 457 (1952). F. Münnich, Naturwissenschaften 42, 340 (1955); E. A. Secco and W. J. Moore, J. Chem. Phys. 23, 1170 (1955); 26, 942 (1957); E. A. Secco, Discuss. Faraday Soc. 28, 94 (1959); E. A. Secco, *Reactivity of Solids* (Wiley, New York, 1969), p. 523; J. P. Roberts and C. Wheeler, Trans. Faraday Soc. 56, 570 (1960); W. J. Moore and E. L. Williams, Discuss. Faraday Soc. 28, 86 (1959); K. S. Kim and B. J. Wuensch, Amer. Ceram. Soc. Bull. 50, 373 (1971); J. W. Hoffmann and J. Lauder, Trans. Faraday Soc. 66, 2346 (1970); R. Robin, A. R. Cooper, and A. H. Heuer, J. Appl. Phys. 44, 3770 (1973); D. Hallwig and H. G. Sockel, *Reactivity of Solids* (Plenum, New York, 1977); H. G. Sockel and D. Hallwig, Mikrochim. Acta Suppl. 7, 95 (1977).
[95]S. Trokman, A. Many. Y. Goldstein, J. Lux, G. Heiland, and D. Kohl, Verh. Dtsch. Phys. Ges. 3, 160 (1980); J. Appl. Phys. (to be published).
[96]E. Spenke, *Elektronische Halbleiter* (Springer, Berlin 1965); W. Shockley and J. S. Last, Phys. 107, 392 (1957).
[97]A. G. Milnes, *Deep Impurities in Semiconductors* (Wiley, New York, 1973); J. S. Blakemore, *Semiconductor Statistics* (Pergamon, New York, 1962).
[98]K. J. Button *et al.*, Phys. Rev. Lett. 28, 1637 (1972).
[99]E. Mollwo, Z. Angew. Phys. 6, 257 (1954).
[100]H. J. Krusemeyer, D. G. Thomas, J. Phys. Chem. Solids 4, 78 (1958).
[101]E. G. Schlosser and W. Herzog, Ber. Bunsenges. Phys. Chem. 71, 358 (1967).
[102]Y. Goldstein and Y. Grinshpan. Phys. Rev. Lett. 39, (15), 953 (1977).
[103]D. Eger and Y. Goldstein, Phys. Rev. B 19, (2), 1089 (1979).
[104]Y. Grinshpan, M. Nitzan, and Y. Goldstein, Phys. Rev. B 19, (2), 1098 (1979).
[105]D. Eger, A. Many, and Y. Goldstein, Surf. Sci. 58, 18 (1976).
[106]See, e.g., G. M. Schwab, and J. Block, Z. Phys. Chem. N. F. 1, 42 (1954); Z. Elektrochem. 58, 756 (1954); U. Doerffler and K. Hauffe, J. Catal. 3, 171 (1964); J. S. Choi and B. W. Kim, Bull. Chem. Soc. Jpn. 46, 21 (1973).
[107]P. Esser, R. Feierabend, and W. Göpel, Conference Proceedings of the Eighth International Vacuum Congress, Cannes, 1980 (in press).
[108]W. Göpel, in *Festkörperprobleme*, edited by J. Treusch (Pergamon Press, New York, 1980), Vol. 20, p. 177.